# Fast light in unbalanced low-loss Mach-Zehnder interferometers

Aida Sánchez-Meroño,[1] María del Mar Sánchez-López,[2] and Julia Arias[1]
[1]*Departamento de Ciencia de Materiales, Óptica y Tecnología Electrónica, Universidad Miguel Hernández, 03202, Elche, Spain*
[2]*Instituto de Bioingeniería, Universidad Miguel Hernández, 03202, Elche, Spain*
(Received 31 January 2014; published 17 April 2014)

An analytical approach is reported that describes previously observed fast-light regimes in linear and passive Mach-Zehnder interferometers (MZI) where the optical path difference is due to a different length of the branches. Approximate expressions are developed for the transmission coefficient and group delay spectral functions valid for frequencies close to the transmission minima $\omega_{\min}$, where these regimes occur. It is found that the group delay at $\omega_{\min}$ verifies a simple scaling law. We demonstrate that slow light cannot arise in this system, and that tunneling and superluminal regimes appear only for low-loss devices, where the attenuation drives the change in the propagation regimes. The propagation of a sinusoidally modulated pulse train through the MZI is described, and relevant figures of merit, which are intrinsic to the system and universal for any operative spectral range, are determined. The theoretical approach is illustrated by simulations of a silicon-based interferometer designed for advancing pulses at 1.55 $\mu$m. Also, previously reported experimental results in the radiofrequency range are interpreted in the framework of the model.

DOI: 10.1103/PhysRevA.89.043828 PACS number(s): 42.25.Bs, 42.25.Hz, 73.40.Gk, 07.60.Ly

## I. INTRODUCTION

Slow and fast light (SFL) technologies are currently receiving much attention because of their interesting applications, ranging from optical information processing, with the realization of optical buffers, quantum memories, switches and synchronizers [1–3], to enhanced precision sensing [4,5] and interferometry [6].

These technologies are based on systems that exhibit steep positive dispersion to propagate a light pulse at unusually low group velocity (slow light, $v_g \ll c$) or steep negative dispersion to achieve pulse propagation at unusually fast group velocity (fast light, $v_g > c$ or negative) [7]. This is the case of materials with gain or absorption resonances [8,9] and of materials where a dip in the gain or in the absorption feature is induced by nonlinear optical processes, like electromagnetic [10] or photo-isomerization-induced [11] transparency, coherent population oscillations [12] or stimulated scattering [13–15]. SFL effects thus arise in a myriad of materials (atomic vapors, solid crystals, dye-doped liquid crystals, semiconductors, and optical fibers) because an abrupt variation of the real part of the complex refractive index (hereafter, simply the refractive index) $n$ occurs in the narrow band around the resonance or dip due to the Kramers-Kronig relations that link the real and imaginary parts of the dielectric function.

Exotic pulse propagation regimes also occur in engineered media without substantial material dispersion, like photonic crystals [16,17] and Bragg gratings [18]. These systems consist of a periodic refractive index distribution and exhibit structural dispersion due to coupling between the incident wavelength and the characteristic length of the structure. The transmission spectrum has a forbidden region for certain directions and polarizations (photonic band gap), which sustains fast light, while slow light is generated at the photonic band edge and at the inside-gap resonance of doped photonic crystals or Bragg gratings. Contrary to the aforementioned systems with material resonances, SFL occurs here in entirely linear and passive structures. Because of the scaling properties of photonic band-gap (PBG) systems, structural SFL has been detected not only in the optical range but also for lower frequencies, like microwave [19–21], radiofrequency (RF) [22,23], and even acoustic wave packets [24].

As an alternative to PBG systems, we recently demonstrated that structural SFL can be generated in multiple-beam interferometers of three or more branches [25,26], which are linear and passive systems not exhibiting photonic band gaps. The simplest interferometer of this kind, with only two branches, is the Mach-Zehnder interferometer. It is a common and versatile device in actual communication systems, widely used to build optical switches [27], modulators for optical signal multiplexing [28], sensors [29], and fractional optical differentiators for pulse-shaping applications and information processing [30]. Its typical interference pattern presents transmission peaks and valleys as a consequence of the phase shift between the two interfering beams, caused by either a difference in the length of the branches (unbalanced or asymmetric MZI), or by a refractive index difference between the branches of equal length (symmetric MZI).

This two-path interferometer has been shown to sustain fast-light propagation for frequencies close to the transmission minima [31–33]. In [31], frequency-domain characterization of an asymmetric loop structure (asymmetric MZI) built with coaxial cables showed negative phase jumps around the transmission minima. This led the authors to point out this structure as a good candidate for obtaining negative group velocity. Time domain experiments performed with Gaussian acoustic pulses [32] and sinusoidally modulated RF wave packets [33] corroborated these findings. By tuning the pulse carrier frequency slightly off the transmission minima, superluminal propagation was also detected [33]. No slow-light regimes were observed. Slow light in an MZI has only been obtained when the medium in one of the branches is microstructured [34] or exhibits a material-resonant feature [35].

The experimental results in [33] were interpreted in the framework of the effective index approach [36]. Within this picture, the scattering loss of the pulse spectral components is

 

ascribed to an effective complex refractive index whose real part is obtained from the overall phase shift on transmission $\phi_t(\omega)$ through the structure. The abrupt negative slope of $\phi_t(\omega)$ at the transmission minima [31–33] causes an anomalous effective dispersion whose origin is structural, i.e., it is not due to dispersion of the medium in the branches (which was, in fact, neglected), but to the features in the spectral transmission. This is also the situation in PBG systems.

In this work we bring these ideas further and develop a theoretical model that fully describes the arising of structural fast light in MZIs and its performance in terms of both the device parameters and the pulse characteristics. The medium in the branches is assumed to be linear and dispersionless in the frequency range of interest, which is a reasonable assumption for a medium exhibiting no gain or absorption peaks. To simplify the analysis, a constant attenuation coefficient is considered, and exact expressions for the complex transmission coefficient and group delay as a function of frequency are obtained. The conditions necessary to obtain appreciable fast light effects are discussed in terms of the fringe visibility, and the allowed propagation regimes are determined as a function of the device characteristics (size, refractive index, and attenuation coefficient of the medium in the branches). We show that the total attenuation is the mechanism that drives the change in the propagation regime for a given refractive index. A substantial difference regarding fast light effects is found between asymmetric and symmetric MZI.

The behavior of a pulse travelling through an SFL system depends not only on the characteristics of the system itself, but also on the pulse shape and duration. As a consequence, the group delay spectral function of the MZI will only be an estimation of the actual pulse delay measured in a time-domain experiment. This issue is addressed in this work by obtaining an approximate expression of the complex transmission coefficient, valid for frequencies close to the transmission minima, that is used to model the propagation of a sinusoidally modulated pulse train through the MZI. An analytic expression of the pulse delay, along with relevant figures of merit that quantify fast-light propagation, is determined. A comparison is made to recently reported SFL effects in three-beam interferometers [25]. The model predictions are illustrated with numerical simulations of a silicon-based MZI designed to operate at optical frequencies. Finally, the previously mentioned experimental results in the RF range [33] are revisited and interpreted in the framework of this model.

## II. ANALYTICAL MODEL

We consider a plane wave of a unit complex amplitude impinging on a Mach-Zehnder interferometer. A $1 \times 2$ splitter divides the wave into two equal components that travel along each arm and then recombine by a $2 \times 1$ coupler. The transmitted complex amplitude at the end of the interferometer is

$$\hat{t} = \frac{1}{2}\sum_{i=1}^{2} e^{j\hat{\phi}_i}, \tag{1}$$

where $\phi_i$ is the phase of the wave propagating along the $i$th branch, which, in turn, can be expressed as

$$\phi_i = \frac{\omega}{\upsilon} L_i + j\alpha L_i. \tag{2}$$

In Eq. (2) $\omega$ is the angular frequency, $\upsilon$ is the phase velocity in the medium, $L_i$ is the $i$th arm length, and $\alpha$ is the attenuation coefficient of the medium. We define the length of each arm as

$$L_1 = L - \frac{\Delta}{2} \quad \text{and} \quad L_2 = L + \frac{\Delta}{2}, \tag{3}$$

where $\Delta$ is the length difference between arms. The effective length of the MZI is the average length of the branches since the input field amplitude is equally split between the two arms

$$L = \frac{(L_1 + L_2)}{2}. \tag{4}$$

Let us define $\beta$ as the phase shift associated to the length difference $\Delta$, i.e., $\beta = \omega\Delta/\upsilon$, and introduce the following quantities:

$$\mathcal{R} = \cosh(\alpha\Delta/2)\cos(\beta/2), \tag{5a}$$

$$\mathcal{I} = -\sinh(\alpha\Delta/2)\sin(\beta/2), \tag{5b}$$

which are related to the transmission coefficient according to $\hat{t} = e^{j(\omega/\upsilon + j\alpha)L}(\mathcal{R} + j\mathcal{I})$.

Therefore, the magnitude and phase of the transmission coefficient can be expressed as

$$|\hat{t}| = e^{-\alpha L}\sqrt{\mathcal{R}^2 + \mathcal{I}^2}, \tag{6a}$$

$$\phi_t = \frac{\beta L}{\Delta} + \arctan\left(\frac{\mathcal{I}}{\mathcal{R}}\right). \tag{6b}$$

The propagation of an electromagnetic pulse through the interferometer is often described in terms of the group delay, which is the time taken by the pulse envelope to propagate through the system [7]. Following the standard stationary phase approach for the plane waves constituting the pulse [19,20], the group delay is obtained from the frequency derivative of the transmission coefficient phase

$$\tau_g = \frac{\partial\phi_t}{\partial\omega} = \frac{L}{\upsilon} + \frac{\mathcal{R}\frac{\partial\mathcal{I}}{\partial\omega} - \mathcal{I}\frac{\partial\mathcal{R}}{\partial\omega}}{\mathcal{R}^2 + \mathcal{I}^2}. \tag{7}$$

Assuming that both the refractive index and attenuation coefficient of the medium in the branches are constant over the whole frequency range of interest, the following expression of the group delay as a function of frequency (through $\beta$) is retrieved

$$\tau_g = \tau_p\left(1 - \frac{\Delta}{2L}\frac{\sinh(\alpha\,\Delta/2)\cosh(\alpha\,\Delta/2)}{\cos^2(\beta/2) + \sinh^2(\alpha\,\Delta/2)}\right), \tag{8}$$

where $\tau_p(= L/\upsilon)$ is the phase delay over the system's effective length. The previous expressions are exact within the assumptions for the medium in the branches. In the following sections, easier to handle approximate equations will be derived with the aim of demonstrating anomalous propagation regimes as well as modeling the propagation of pulses through the MZI. The conditions considered for such a derivation are now discussed.

First, the analysis will be centered in a narrow frequency region around the transmission minima since it is where

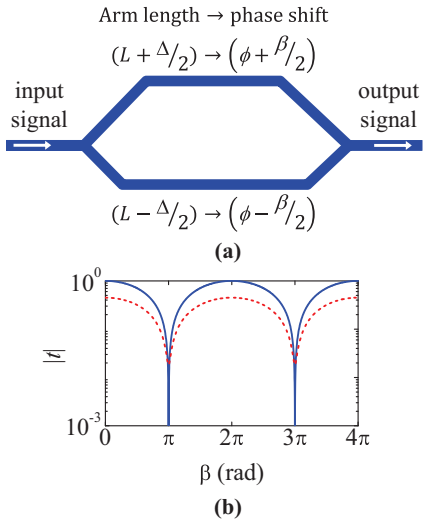


FIG. 1. (Color online) (a) Schematic of an unbalanced MZI and (b) its typical transmission spectrum with (dashed line) and without (solid line) attenuation.

fast light was experimentally observed [31–33]. An MZI has one minimum between two adjacent principal peaks on transmission. The extrema of the transmission function $|\hat{t}(\beta)|$ of Eq. (6a) lie at phase values $\beta_{\min} = (2m+1)\pi$ (for minima) and $\beta_{\max} = 2\pi m$ (for maxima), where $m$ is an integer number. The position of the minima does not change with attenuation, in contrast to the situation in a three-beam interferometer [25]. A schematic of the two-beam interferometer and its transmission spectrum with and without attenuation are displayed in Fig. 1.

Second, our analytical approach will be performed within the condition of high fringe contrast of the interference pattern (i.e., weak attenuation), which is necessary for the arising of anomalous pulse propagation regimes. In the absence of attenuation ($\alpha = 0$), Eq. (8) yields $\tau_g = \tau_p$, as it is expected in a linear and lossless system, where the phase relation between the pulse components remains unchanged and consequently the pulse peak travels at the phase velocity. On the opposite case, for very high attenuation, no anomalous pulse propagation regimes are observed. Since a high attenuation reduces the contrast of the interference pattern (as it can be appreciated in Fig. 1), the present analytical study will be performed within the condition of good visibility of the fringes. Such a condition corresponds to considering small $\alpha\Delta$ values, as it is demonstrated below.

The visibility of the interference pattern (or fringe contrast) is defined as [35]

$$\nu \equiv \frac{T_{\max} - T_{\min}}{T_{\max} + T_{\min}}, \tag{9}$$

where $T = |\hat{t}|^2$ is the transmittance and the subscript indicates its maximum or minimum value. Considering the phase values of the transmittance extrema ($\beta_{\max}$ and $\beta_{\min}$) into Eqs. (5) and (6), the fringe contrast of the MZI is found to depend solely on the attenuation along the length difference between branches ($\alpha\Delta$)

$$\nu \equiv \frac{2e^{-\alpha\Delta}}{1+e^{-2\alpha\Delta}}, \tag{10}$$

For a lossless interferometer ($\alpha = 0$) one gets $\nu = 1$, whereas the losses decrease the fringe visibility; the higher $\alpha\Delta$, the smaller is the fringe contrast. Since fast-light effects requires sharp spectral features, a visibility of at least $\nu = 0.65$ is required [35], and this requires that the amplitude ratio of the combining waves at the end of the MZI, $e^{-\alpha\Delta}$, should be less than $1/e$, that is, $\alpha\Delta < 1$. The analytical approximation in the next section will consider $\alpha\Delta < 0.5$ values, which assures a very good fringe visibility ($\nu \geqslant 0.9$) along with excellent agreement with the exact model developed above.

### A. Transmission coefficient and group delay *around* the transmission minima

Let us derive approximate equations of the magnitude $|\hat{t}(\omega)|$ and phase $\phi_t(\omega)$ of the transmission coefficient, and the group delay $\tau_g(\omega)$, valid for frequencies close to a transmission minimum $\omega_{\min}$. These expressions will be used in Sec. II C to study the propagation of narrowband sinusoidally modulated pulses through the MZI.

The transmission coefficient in Eq. (6) can be written in the terms of $(\beta - \beta_{\min})$. After some algebraic operations, the following expressions are obtained:

$$|\hat{t}| = e^{-\alpha L}\sqrt{\sin^2\left(\frac{\beta-\beta_{\min}}{2}\right) + \sinh^2\left(\frac{\alpha\Delta}{2}\right)}$$
$$\approx e^{-\alpha L}\sqrt{\left(\frac{\beta-\beta_{\min}}{2}\right)^2 + \left(\frac{\alpha\Delta}{2}\right)^2}, \tag{11a}$$

$$\frac{\mathcal{I}}{\mathcal{R}} = \frac{\tanh(\alpha\Delta/2)}{\tan(\beta-\beta_{\min}/2)} \approx \frac{\alpha\Delta}{\beta-\beta_{\min}}, \tag{11b}$$

where the approximation valid for small angles $(\beta - \beta_{\min})$ and small $\alpha\Delta$ was considered. Recalling that $\beta = \omega\Delta/\upsilon$ and defining a new parameter $\gamma = -\alpha\upsilon$, this leads to the following approximate equations for the magnitude and phase of the transmission coefficient around the minima $\omega_{\min}$

$$|\hat{t}(\omega)| \approx e^{-\alpha L}\frac{\alpha\Delta}{2}\sqrt{1+\left(\frac{\omega-\omega_{\min}}{\gamma}\right)^2}, \tag{12a}$$

$$\phi_t(\omega) \approx \omega\tau_p + \arctan\left(\frac{\omega-\omega_{\min}}{\gamma}\right) + \frac{\pi}{2}. \tag{12b}$$

Note that the result of null transmission at the minima is recovered for the lossless case ($\alpha = 0$). Finally, the approximate expression for the group delay around each transmission minimum is retrieved through a $\omega$ derivation of the phase function in Eq. (12b)

$$\tau_g(\omega) \approx \tau_p + \frac{\gamma}{(\omega-\omega_{\min})^2 + \gamma^2}. \tag{13}$$

Equation (13) shows that the *excess* group delay $(\tau_g - \tau_p)$ around the minima is a Lorentzian function, with $|\gamma|$ the half-width at half maximum (HWHM) and $1/\gamma$ the excess group delay at the transmission minima. Since $\gamma$ is directly proportional to the attenuation coefficient for a given refractive index, one concludes that the larger the losses, the wider will be the group delay Lorentzian curve and the smaller will be the group delay absolute value at $\omega_{\min}$. Hence, the softening

of the anomalous propagation regimes when the losses in the system are notable is proved.

### B. Pulse propagation regimes *at* the transmission minima

In this section we provide theoretical proof that tunneling and superluminal regimes can arise at the transmission minima by properly choosing the interferometer's effective length for a given attenuation coefficient and refractive index. From Eq. (8) the exact group delay at the transmission minima $\beta_{\min}$ reads

$$\tau_g = \tau_p \left[ 1 - \frac{\Delta}{2L} \coth\left(\frac{\alpha\Delta}{2}\right) \right], \tag{14a}$$

which can be approximated for small values of $\alpha\Delta$ as

$$\tau_g \approx \tau_p \left(1 - \frac{1}{\alpha L}\right) = \tau_p + \frac{1}{\gamma}. \tag{14b}$$

Alternatively, the above expression could also be obtained by evaluating Eq. (13) at $\omega_{\min}$.

Interestingly, if we now apply the relationship between the attenuation coefficient and the imaginary part of the complex refractive index $n_i$ ($\alpha = n_i\omega/c$) into Eq. (14b), the group delay at $\omega_{\min}$ can also be approximated as

$$\tau_g \approx \tau_p - \frac{n}{n_i}\frac{1}{\omega_{\min}}. \tag{14c}$$

The above expression brings two interesting points into attention. First, it sets a scaling law for the group delay since it indicates that the product $\omega_{\min} \times (\tau_g - \tau_p)$ does not depend on the interferometer's operative frequency range, but only on the ratio between the real and imaginary parts of the complex refractive index of the medium in the branches ($n/n_i$). Second, equivalent expressions were obtained for the group delay at the reflection minima of a weakly absorbing dielectric slab [21,37], which is indeed a multibeam interferometer. Therefore, it shows the resemblance between pulse transmission through an MZI and pulse reflection on a dielectric slab. This should not be unexpected since the MZI transmission spectrum is, in fact, very similar to the dielectric slab reflection spectrum.

Following the discussion, we now focus on a system with a given refractive index and take Eq. (14b) to analyze the possible propagation regimes at the minima. Equation (14b) shows that a lossy MZI cannot sustain slow light ($\tau_g$ cannot be larger than $\tau_p$) because $\alpha$ is positive by definition. Only in the hypothetical case of an interferometer with gain ($\alpha < 0$) would the subluminal regime arise. Practical situations, like considering an MZI with a medium in one of the branches that exhibits a narrow gain resonance, are discussed in the literature [35].

The interferometer will sustain tunneling at the minima ($\tau_g < 0$) if the attenuation coefficient and the effective length are chosen so that

$$\alpha L < 1. \tag{15}$$

For larger $\alpha L$, the superluminal regime will arise ($0 < \tau_g < L/c$) if the following condition is satisfied:

$$1 < \alpha L < \frac{n}{n-1}. \tag{16}$$

TABLE I. Possible propagation regimes at the transmission minima for a lossy MZI.

| Condition | $\alpha L < 1$ | $1 < \alpha L < \frac{n}{n-1}$ | $\alpha L > \frac{n}{n-1}$ |
|---|---|---|---|
| $\alpha > 0$ | Tunneling | Superluminal | Normal |

Therefore, the change in the pulse propagation regime is driven by the total attenuation of the interferometer $\alpha L$, which can be modified by either changing the medium in the branches (i.e., $\alpha$) and/or the interferometer's effective length $L$. The length difference between branches $\Delta$ plays no role in this issue, it only determines the frequency position of the minima, namely $\omega_{\min} = (2m+1)\pi v/\Delta$. Table I summarizes the possible propagation regimes at the minima as a function of $\alpha L$.

The above analysis is illustrated by performing numerical simulations on a silicon-based MZI with refractive index $n = 3.48$. Figure 2 shows, for two attenuation values and $\Delta = L/10$ the magnitude of the transmission coefficient calculated using Eq. (6a) and the group delay as a function of $\beta$ according to Eq. (8). As it was discussed, no anomalous propagation regimes occur in the lossless interferometer, while if losses with $\alpha\Delta = 0.015$ are considered, tunneling arises at each minimum with negative group delays close to $-6\tau_p$.

Figure 3 shows how the system's total attenuation drives the change in the pulse propagation regime. The group delay at the minima (normalized to the phase delay) is plotted as a function of $\alpha L$ for an interferometer with $\alpha\Delta = 0.015$. Together with the $\tau_g$ values obtained from Eq. (14a), the straight line $1/n$ corresponding to propagation over length $L$ in a vacuum is represented. The system exhibits negative group delays for small-enough attenuation ($\alpha L < 1$). For values of $\alpha L$ ranging between 1 and 1.4, the propagation is superluminal,

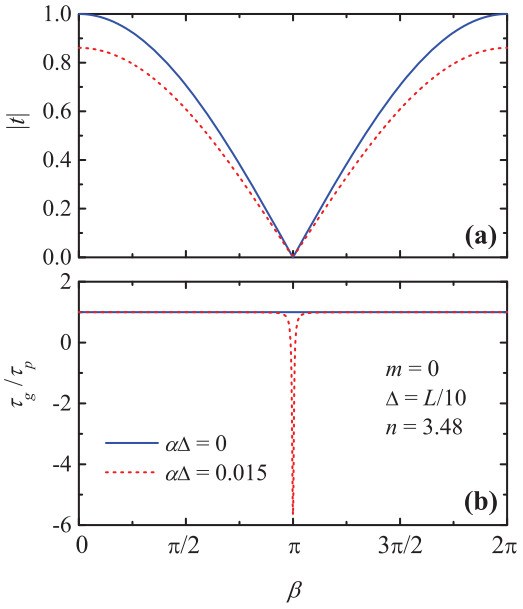


FIG. 2. (Color online) (a) Transmission coefficient magnitude and (b) group delay in units of phase delay through an Si-based MZI with length difference between arms $\Delta = L/10$ and refractive index $n = 3.48$ for two values of the attenuation coefficient $\alpha$.

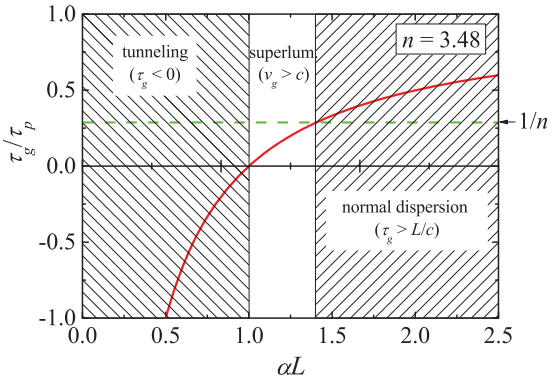


FIG. 3. (Color online) Pulse propagation regimes at the transmission minima of an Si-Based MZI with $\alpha\Delta = 0.015$ as a function of the total attenuation $\alpha L$. Group delay plotted from Eq. (14a) (solid line) and phase delay through a vacuum (dashed line). The delays are given in units of the phase delay over the system's effective length.

in agreement with Eq. (16), while for too high attenuation $\alpha L > 1.4$ normal propagation is obtained. Therefore, fast light is achieved for weak-enough attenuation, while it disappears if it is either zero or too high ($> \frac{n}{n-1}$).

The fast-light conditions summarized in Table I and the impossibility of getting slow light coincide with those obtained for a three-beam interferometer with constant length difference $\Delta$ between adjacent arms [25]. In fact, the exact expression of the group delay at the transmission minima of this latter system is the same as the one derived here if $\Delta$ in Eq. (14a) is substituted by $2\Delta$, i.e., the length difference between the shortest and the longest arms of the three-beam interferometer. Therefore, a three-beam interferometer with constant $\Delta$ behaves, as far as SFL effects are concerned, as an MZI.

### C. Propagation of sinusoidally modulated pulses

The propagation of a pulse train through the MZI is now modeled. A sinusoidally modulated wave packet with carrier frequency $\omega_c$ and modulation frequency $\omega_m$ is considered, $E_{\text{in}}(t) = E_c \sin(\omega_c t)[1 + M_{\text{in}}\cos(\omega_m t)]$, where the modulation index $M_{\text{in}}$ is the amplitude ratio of the modulating and carrier signals. Together with the carrier component, this kind of modulation generates two side components of amplitude $E_{\pm s} = M_{\text{in}}E_c/2$ and frequencies $\omega_{\pm s} = \omega_c \pm \omega_m$. By setting the carrier frequency at one of the minima ($\omega_c = \omega_{\min}$) and using Eq. (12), the amplitude and phase of each spectral component after propagating through the system are obtained. Using Fourier theory, the envelope of the pulse transmitted through the interferometer reads

$$E_{\text{out}}(t) \propto 1 + M_{\text{out}}\cos[\omega_m(t - \tau_{\text{pulse}})], \tag{17}$$

with modulation index ($M_{\text{out}}$) and delay ($\tau_{\text{pulse}}$) of the output pulse given by

$$M_{\text{out}} = M_{\text{in}}\sqrt{1 + \left(\frac{\omega_m}{\gamma}\right)^2}, \tag{18}$$

$$\tau_{\text{pulse}} = \tau_p + \frac{1}{\omega_m}\arctan\left(\frac{\omega_m}{\gamma}\right), \tag{19}$$

keeping in mind that $\tau_p = L/\upsilon$ and $\gamma = -\alpha\upsilon$.

The pulse delay in Eq. (19) is the time that a sinusoidally modulated pulse train of modulation frequency $\omega_m$ and a carrier frequency tuned at $\omega_{\min}$ takes in travelling through the MZI. In the limit of extremely narrow pulse bandwidth $\omega_m \to 0$, $\tau_{\text{pulse}} \to \tau_p + 1/\gamma$, thus recovering the group delay value at $\omega_{\min}$ which was discussed in Sec. II B. In other words, this analysis shows that the narrower the spectral pulse width, the more the *pulse delay* measured in a time-domain propagation experiment approaches the value of the *group delay* given by Eq. (14a).

An important figure of merit in SFL systems is the fractional delay [38], $D_f$, defined as the ratio between the excess pulse delay and the duration of the incident pulse $T_{\text{in}}$:

$$D_f = \frac{\tau_{\text{pulse}} - \tau_p}{T_{\text{in}}}. \tag{20}$$

This quantity is equal to the excess number of pulses that can be contained at any time within the system with respect to the number that would be contained if the pulses travelled at the phase velocity. It is hence a measure of how much the information storage capacity of the system is enhanced due to SFL effects. A common definition when dealing with optical pulses is to take the pulse duration as the FWHM of the pulse power. For sinusoidally modulated pulses of modulation index $M$, the pulse duration is $T = 2/\omega_m \arccos((1 - \sqrt{2} + M)/\sqrt{2}M)$ and consequently, $D_f$ reads

$$D_f = \frac{\arctan\left(\frac{\omega_m}{\gamma}\right)}{2\arccos\left(\frac{1-\sqrt{2}+M_{\text{in}}}{\sqrt{2}M_{\text{in}}}\right)}. \tag{21}$$

Figure 4(a) shows that the fractional advancement $|D_f|$ (solid line) increases with modulation frequency. Also, Eq. (21) predicts $|D_f| = 34\%$ if modulation is performed with $M_{\text{in}} = 1$ and $\omega_m = |\gamma|$, i.e., the pulse spectral components lie within the FWHM of the group delay function in Eq. (13). For higher modulation frequencies, however, the pulse will undergo a certain degree of distortion, which is larger as $\omega_m$ increases. According to Eq. (18), the modulation index of the transmitted pulse is always larger than that of the input pulse, and consequently, the duration of the output pulse ($T_{\text{out}}$) will always be smaller, leading to a pulse compression $b$, whose value can be calculated by

$$b = 1 - \frac{T_{\text{out}}}{T_{\text{in}}} = 1 - \frac{\arccos\left(\frac{1-\sqrt{2}+M_{\text{out}}}{\sqrt{2}M_{\text{out}}}\right)}{\arccos\left(\frac{1-\sqrt{2}+M_{\text{in}}}{\sqrt{2}M_{\text{in}}}\right)}. \tag{22}$$

Figure 4(a) shows (dashed line) the relation between pulse compression and modulation frequency (normalized to $|\gamma|$). It is found that for not too high values of $\omega_m$ the compression factor goes roughly quadratic with the fractional delay $b \approx K D_f^2$. Considering $M_{\text{in}} = 1$, the proportionality constant $K$ is 0.74 if $\omega_m \to 0$ and it is 0.71 if $\omega_m = |\gamma|$. This relation is illustrated in Fig. 4(b); it implies that, to keep the pulse compression below 5%, the fractional delay may not exceed 27%, and to keep it below 10% the fractional delay may not exceed 38%.

In addition to pulse compression, distortion of the pulse amplitude also appears, similarly to what is observed for fast light in systems with material resonances [39]. In the case of $M_{\text{in}} = 1$, this amplitude distortion acts as a pulse breakup, giving

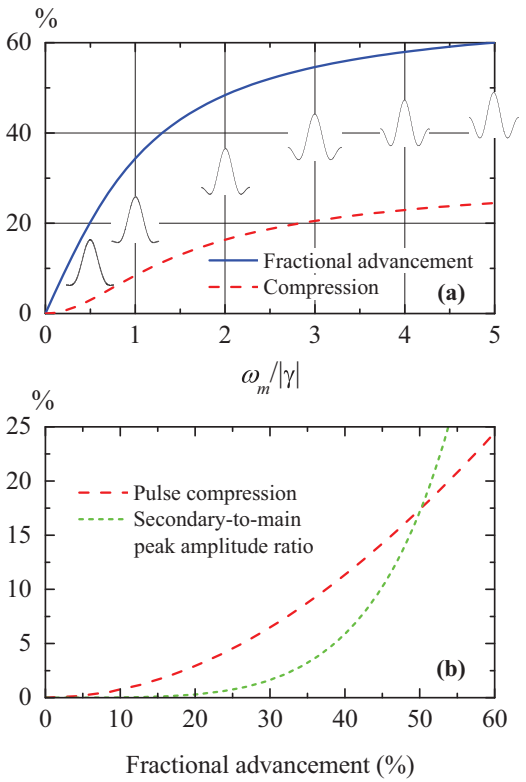


FIG. 4. (Color online) (a) Fractional advancement (solid line) and pulse compression (dashed line) versus normalized modulation frequency, and (b) pulse compression (dashed line) and secondary to main peak amplitude ratio (short-dashed line) as a function of the fractional advancement, for a 100% sinusoidally modulated pulse train with carrier frequency tuned at one of the transmission minima.

rise to a main peak (lying at $t = \tau_{\text{pulse}}$) and a secondary peak (lying at $t = \tau_{\text{pulse}} + \pi/\omega_m$). The secondary-to-main power amplitude ratio is given by $(1 - M_{\text{out}})^2/(1 + M_{\text{out}})^2$, which increases with increasing modulation frequency, or equivalently, with increasing fractional advancement, as shown in Fig. 4(b). Thus, to maintain the secondary peak amplitude below 10% of the main peak amplitude, the fractional delay may not exceed 45%.

Another relevant figure of merit of SFL systems is the delay-bandwidth product (DBP) [38], defined as the product of the delay and bandwidth of the signal transmitted through the system. This quantity can be estimated in various units depending on which magnitude the bandwidth is given. Choosing a modulation frequency $f_m = |\gamma|/2\pi$ so that the spectral components of the signal here considered lie within the FWHM of the Lorentzian group delay curve in Eq. (13), the expected DBP is $(\tau_{\text{pulse}} - \tau_p) \times 2 f_m = 25\%$.

It is worth noticing that the above features and figures of merit are entirely applicable to MZIs operating at any frequency range. In this context, we shall recall the simple scaling law for the excess group delay at $\omega_{\text{min}}$ that was previously obtained [see Eq. (14c)], which is useful to transform a device originally designed to operate at a specific frequency range into another operative range. Finally, let us point out that the pulse propagation characteristics described above are equivalent to those derived for a three-beam interferometer [25].

## III. RESULTS AND DISCUSSION

In this section, the model predictions are applied to Mach-Zehnder interferometers operative at two different spectral regions. First, a numerical simulation of the propagation of optical pulses centered at 1.55 $\mu$m is performed and second, our previous experimental results obtained in the RF range are revisited and interpreted in the framework of the model.

### A. Simulation results in the optical range

A silicon-based MZI with an attenuation coefficient of 6.5 dB/cm and a refractive index of $n = 3.48$ is considered. It is designed to have a fixed branch length difference of $\Delta = 200\mu$m that sets the minima 430 GHz apart. Therefore, the model parameters take the values $\alpha\Delta = 0.015$ and $\gamma^{-1} = -155$ ps. The conditions summarized in Table I yield the range of values that the system's effective length $L$ must take to sustain tunneling, superluminal, or normal group delay at the minima. Consequently, three such MZIs of the following lengths are considered: $L = 2$ mm (tunneling), $L = 1.5$ cm (superluminal), and $L = 2$ cm (normal).

The transmission magnitude $|\hat{t}|$ and group delay $\tau_g$ of the three MZIs are calculated according to Eqs. (6a) and (8) in a frequency range of 450 GHz centered at the transmission minimum located at $f_{\text{min}} \approx 193$ THz; the results are plotted in Fig. 5(a). As $L$ increases, the attenuation of the transmission

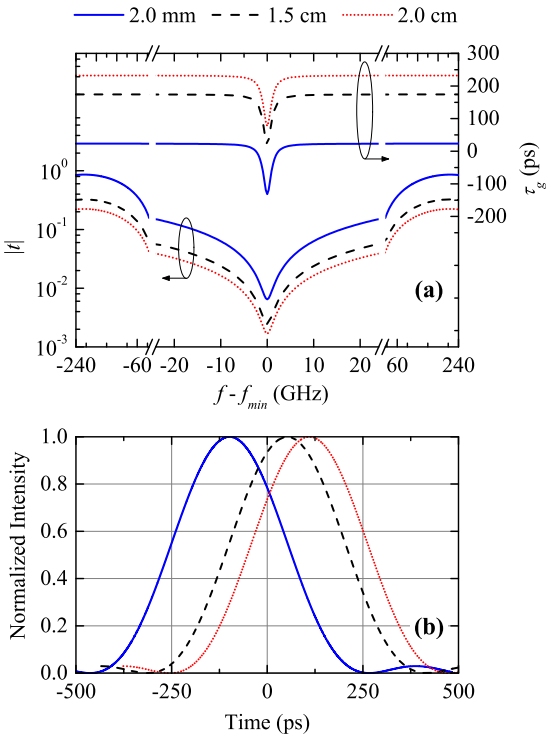


FIG. 5. (Color online) Numerical simulation of an Si-based MZI with parameters $\Delta = 200$ $\mu$m, $\alpha = 6.5$ dB/cm, and $n = 3.48$ for three values of the effective length: $L = 2$ mm (solid line), $L = 1.5$ cm (dashed line), and $L = 2$ cm (dotted line). (a) Magnitude of the transmission coefficient and group delay. (b) Normalized traces of pulses with carrier frequency tuned at $f_{\text{min}}$ and transmitted through each interferometer. The incident pulse has its peak at $t = 0$.

spectrum becomes stronger and the group delay curve shifts upwards because of the positive contribution of a larger phase delay. The group delay value at $f_{\min}$, namely $\tau_g \approx -131, 19,$ and 77 ps, corresponds to the tunneling, superluminal, and normal regimes, respectively, in agreement with the model predictions. For each interferometer, the excess group delay curve $\tau_g(f) - \tau_p$ fits excellently to a Lorentzian function of HWHM $|\gamma|/2\pi \approx 1$ GHz and $-155$ ps excess delay at the minimum.

Now, an optical pulse train travelling through each interferometer is numerically simulated. The optical carrier is tuned at $f_{\min} \approx 193$ THz ($\lambda = 1.55\,\mu$m) and it is 100% sinusoidally modulated at frequency $f_m = |\gamma|/2\pi$ to generate a train of pulses of width $T_{\text{in}} = 364$ ps at a repetition rate of 1 GHz. Figure 5(b) shows the pulse traces corresponding to a propagation through the interferometers of $L = 2$ mm (pulse 1), $L = 1.5$ cm (pulse 2), and $L = 2$ cm (pulse 3). All traces were normalized to its peak value for an easier comparison. The peak position of each envelope is the time that the pulse takes in travelling through the system, i.e., the pulse delay. These delays are, respectively, $\approx -98, 52,$ and 110 ps and they agree very well with the values predicted by Eq. (19). Since the incident pulse (not depicted) has its peak at $t = 0$, pulse 1 clearly tunnels through the system, pulse 2 propagates almost superluminally (the superluminal delay should be less than $L/c = 50$ ps), whereas pulse 3 corresponds to a normal propagation. For the three pulses shown in the figure, a fractional advancement of $|D_f| = 34\%$ was observed, in agreement with Eq. (21).

The case of pulse 2 is a neat example that Table I provides an *estimation* of the propagation regime for narrowband pulses tuned at the minima. The pulse spectral width has indeed influence on the actual propagation regime, as it is reflected in Eq. (19) for $\tau_{\text{pulse}}$. It was checked that by decreasing the modulation frequency slightly below 1 GHz, the resulting pulse does propagate superluminally through the MZI of $L = 1.5$ cm.

Figure 6 shows the normalized traces of two pulses transmitted through the shortest MZI ($L = 2$ mm, and phase delay $\tau_p = 23$ ps) and tuned at two frequencies: $f_{\min} \approx 193$ THz

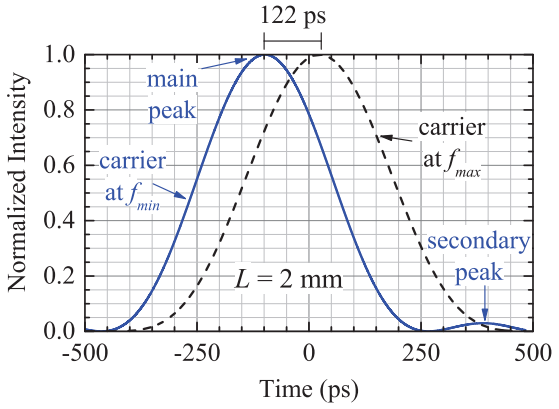


FIG. 6. (Color online) Normalized traces of pulses transmitted through the interferometer of $L = 2$ mm for two carrier frequencies: tuned at $f_{\min}$ (solid line) and tuned at $f_{\max}$ (dashed line). The incident pulse has its peak at $t = 0$.

(pulse 1) and the next transmission maximum $f_{\max} = f_{\min} + 215$ GHz. Since the pulse with carrier frequency at $f_{\max}$ travels at the phase velocity, pulse 1 (main peak) is advanced 121 ps with respect to it. A slight compression of pulse 1 is revealed by measuring the widths of both pulses. Such a compression also occurs for pulse 2 and pulse 3 shown in the previous figure. In the three cases a compression factor of $b = 8\%$ is observed, in agreement with Eq. (22). In physical terms, this behavior can be ascribed to spectral reshaping of the input pulse due to the transmission feature at the minimum. Namely, the center pulse frequency is transmitted with less intensity that its side components, thus causing spectral broadening, and consequently, pulse shrinking in time. This situation has also been reported for fast light based on material resonances [39].

Figure 6 also shows the pulse 1 breakup, with a discernible secondary peak at 388 ps and power amplitude of 2.9% of the main peak power amplitude, in excellent agreement with the predicted values given that $M_{\text{out}} = \sqrt{2}$.

It is worth emphasizing that the above numerical simulations regard an *ideal* waveguide silicon-based MZI. Real waveguide-integrated interferometers usually have power imbalance on the nominal 3 dB couplers [27]. Interestingly, power imbalance can play the role of total losses $\alpha L$ in changing the propagation regime, as it can be deduced from the results found in [30]. In that work, the author analyzed the performance of an MZI with variable power splitting ratios. The softening of the phase jump in the phase spectral function for splitting ratios detuning from 3 dB is similar to the effect of total losses.

For practical purposes, one might consider the possibility of inducing the optical path difference in the MZI not by means of a physical length difference $\Delta$, but through a difference in the refractive index of the branches $\Delta_n$. We could then envisage an MZI with equal branch lengths and fabricated using an electro-optic material such as $LiNbO_3$, where $\Delta_n$ is tuned upon the application of voltage [27]. It must be pointed out though that SFL effects cannot occur in such a device. More specifically, in an MZI with branches of equal length (and equal attenuation coefficient), the transmission is exactly zero at the minima for whatever attenuation coefficient. The plane-wave amplitude at the end of each branch is the same, and $\Delta_n$ makes the phase shift between each plane wave an odd multiple of $\pi$ for certain frequencies, thus completely cancelling the transmission at those frequencies. No degree of freedom is left to yield an anomalous propagation regime. This situation is equivalent to that of the asymmetric and lossless MZI shown in Sec. II, which displays zero transmission at the minima and $\tau_g = \tau_p$. This physical discussion can be readily corroborated by a simple calculation for this hypothetical symmetric interferometer; it leads to a group delay that corresponds to a propagation at the average phase velocity, namely $\tau_g = \bar{n}L/c$, with $\bar{n}$ being the average refractive index of the branches.

### B. Revisiting experimental results in the RF range

The experimental results reported in our previous work [33] are now analyzed within the framework of the present model. The interferometer consists of two coaxial cables (50 Ω, RG-58C/U) of 2 and 14 m length, connected by a $1 \times 2$ RF power splitter and a $2 \times 1$ RF coupler (PE2000 Pasternack).

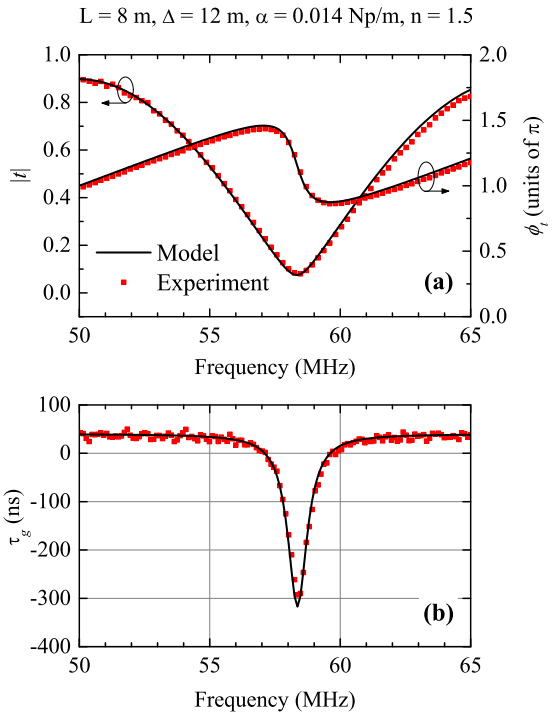


FIG. 7. (Color online) Experimental and model results of an RF MZI with the indicated parameters around a transmission minimum. (a) Magnitude and phase of the transmission coefficient and (b) group delay.

Hence, the system's effective length is $L = 8\,\text{m}$ and $\Delta = 12\,\text{m}$ is the length difference between branches. The phase velocity in the cables ($\upsilon = 2c/3$) corresponds to a refractive index of $n = 1.5$. The phase delay of the system is thus $\tau_p = 40\,\text{ns}$. The cable attenuation coefficient was characterized as a function of frequency in the 20–100 MHz range yielding an average value of $\alpha = 0.014\,\text{Np/m}$, which is considered as the constant coefficient loss in the model equations. Therefore, the model parameters take the values $\alpha\Delta = 0.168$ and $\gamma^{-1} = -1/\alpha\upsilon = -357.14\,\text{ns}$. Considering Table I and the fact that $\alpha L = 0.112 < 1$, tunneling is the predicted group delay regime at the transmission minima. This regime should be clearly noticeable since the fringe visibility is $\nu = 99\%$.

The transmission magnitude, $|\hat{t}|$, the phase on transmission, $\phi_t$, and the group delay $\tau_g$ of this MZI were calculated using Eqs. (6a), (6b), and (8). They are plotted in Fig. 7 together with previous experimental results [33] for comparison. The experimental $|\hat{t}|$ and $\phi_t$ curves correspond to the magnitude and phase of the $S_{21}$ scattering parameter, which was recorded with a two-port vector network analyzer (Agilent E8363B) in the 20–100 MHz range every 112.5 kHz. The experimental $\tau_g$ curve was retrieved by numerical derivative of the experimental phase data with respect to the frequency. It should be remarked that in the experimental data shown here, the effects of the splitters (an overall attenuation of 1dB and a delay of 2 ns) were subtracted since the splitters are not included in the model. As Fig. 7(a) shows, the constant loss coefficient $\alpha = 0.014\,\text{Np/m}$ considered in the model fits very well the experimental $|\hat{t}|$ and $\phi_t$ curves in the displayed frequency range. The experimental transmission minimum lies at 58.3625 MHz, i.e., 62.5 kHz above the theoretical $f_{\min}$. The agreement was found to be also good in a broader spectral range (20–100 MHz), with the only effect of a lowering of the measured transmission peaks for larger frequencies because of the frequency dependence of the actual coefficient loss.

As shown in Fig. 7(b), the experimental group delay function is reasonably well accounted for by the theoretical model. The experimental and theoretical group delay at the minimum takes the values $\tau_g^{\text{expt}}(f_{\min}) = -292.81\,\text{ns}$ and $\tau_g^{\text{theor}}(f_{\min}) = -316.46\,\text{ns}$, respectively. The error in the experimental value is estimated to be $\pm 30\,\text{ns}$, considering the data experimental dispersion and the frequency discretization. Let us note that the frequency derivative of the phase data amplifies the small amount of noise that is contained in the measured $S_{21}$ parameter; this is why the experimental $\tau_g^{\text{expt}}$ curve exhibits significant data dispersion. The theoretical prediction of $-316.46\,\text{ns}$ lies within the experimental range $\tau_g^{\text{expt}}(f_{\min}) = -292.81 \pm 30\,\text{ns}$. It is worth mentioning that the Lorentzian approximation of Eq. (13) with model parameter $\gamma^{-1} = -357.14\,\text{ns}$ almost perfectly fits the experimental function $\tau_g^{\text{expt}}(f)$.

The above results are now used to interpret the time-domain experiments reported in [33], where a train of sinusoidally modulated wave packets with carrier frequency in the megahertz range and 500 kHz modulation frequency was transmitted through the system. This modulation frequency is only by ≈50 kHz larger than $|\gamma|/2\pi$. Consequently, the side spectral components of the pulse lie only slightly beyond the FWHM of the Lorentzian group delay curve. Figure 8 shows the experimental pulse power traces (normalized to their maximum value) and their fitted envelopes for two different carrier frequencies $f_c$. A pulse delay of $-250 \pm 40\,\text{ns}$ was reported for the wave packet with carrier frequency tuned at 58.3 MHz; i.e., it tunnels through the system since $t = 0$ is the peak position of the incident pulse. The pulse with

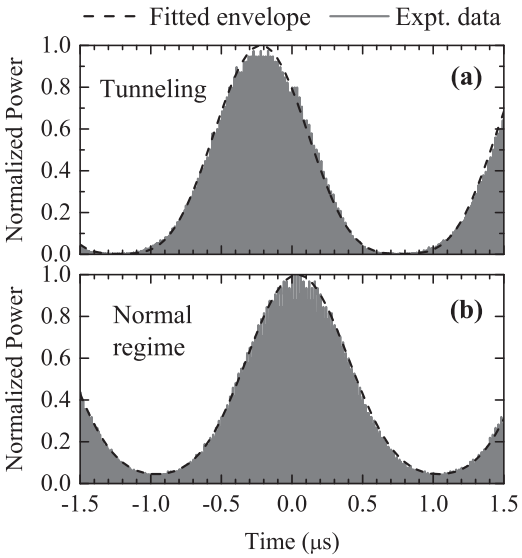


FIG. 8. Experimental pulse power traces and their fitted envelopes for two different carrier frequencies: (a) 58.3 MHz (tunneling) and (b) 50 MHz (normal regime). Each trace is normalized to its maximum amplitude. The fitted envelopes have modulation index (a) $M = 0.95$ and (b) $M = 0.65$.

TABLE II. Comparison between experimental and theoretical predictions for a tunnelled pulse in the RF MZI under analysis. The experimental data of Ref. [33] were used.

| Results | $M_{\text{out}}$ | $\tau_{\text{pulse}}$(ns) | $\lvert D_f \rvert$ | $b\%$ |
|---|---|---|---|---|
| Experiment | $0.95 \pm 0.05$ | $-250 \pm 40$ | $0.35 \pm 0.05$ | $11.4 \pm 1.3$ |
| Theory | 0.98 | $-228$ | 0.32 | 12.2 |

$f_c = 50\,\text{MHz}$ is delayed by 40 ns and undergoes neither distortion nor compression. This allows us to take the features of this pulse as those of the input pulse in our model. It also serves as the reference pulse for estimating the phase delay $\tau_p$ (40 ns) since its propagation is equivalent to that of a pulse traversing a single coaxial cable of 8 m (the MZI effective length). The envelopes that fit the experimental captures have modulation index $M_{\text{out}} = 0.95 \pm 0.05$ [Fig. 8(a)] and $M_{\text{in}} = 0.65$ [Fig. 8(b)]. Let us remark that because of the higher distortion of the tunnelled pulse (due to the sharp decrease of the transmitted signal at the minima) a rough error of $\pm 0.05$ was estimated in its modulation index. Using the above values of the modulation index, the pulse duration (FWHM) for the tunnelled and input pulses is $T_{\text{out}} = 739.5 \pm 11.5\,\text{ns}$ and $T_{\text{in}} = 835\,\text{ns}$.

Table II summarizes the comparison between the model predictions and the experimental results for the following quantities of the tunnelled pulse: output modulation index $M_{\text{out}}$, pulse delay $\tau_{\text{pulse}}$, fractional delay $D_f$, and compression factor $b$. The theoretical predictions were obtained using $\omega_m = 2\pi \times 500\,\text{kHz}$ and the model parameter $\gamma^{-1} = -357.14\,\text{ns}$ into Eqs. (18), (19), (21), and (22). The experimental value of $D_f$ was obtained from Eq. (20) using $\tau_{\text{pulse}}^{\text{expt}} = -250 \pm 40$ ns. The experimental figures of merit bear a good agreement with the model predictions. Since the output modulation index is $M_{\text{out}} \leqslant 1$ (as a consequence of having $M_{\text{in}} = 0.65$) no peak breakup is observed, in accordance to the theory.

## IV. CONCLUSION

We have theoretically proved the arising of structural fast light in a linear, passive, weakly attenuating, unbalanced MZI. The interferometer is characterized by its branch length difference ($\Delta$), its effective length ($L$), and the refractive index ($n$) and attenuation coefficient ($\alpha$) of the medium in the branches, which are both considered constant.

An approximate analysis is performed within the condition of good fringe visibility (small $\alpha\Delta$) and in a narrow spectral region around the transmission minima, where anomalous regimes are observed. The intensity of fast-light regimes depends on how much the group delay differs from the phase delay, i.e., the *excess* group delay. It is highlighted that the magnitude of the excess group delay at the transmission minima scales with frequency by a proportionality constant, which is the ratio between the real and the imaginary parts of the complex refractive index of the branch media, in the same way as it has been reported for other interferometric systems; namely for pulses reflected on weakly absorbing slabs.

Keeping constant the refractive index, it is demonstrated that the total attenuation of the system $\alpha L$ drives the change in the group delay regimes at the minima, which range from tunneling, to superluminal, and finally, into normal regime as $\alpha L$ increases. Similar to other structural SFL systems, the obtained group delay spectral function is very well approximated by a Lorentzian curve in the frequency region around the transmission minima.

The propagation of amplitude-modulated sinusoidal pulses through an MZI is modeled and typical figures of merit intrinsic to the system have been obtained. Pulse advancement comes at the expense of pulse compression, and under certain modulation conditions, also peak-breakup. For a 100% modulated pulse with its entire spectrum within the Lorentzian group delay function the delay-bandwidth product is 25% and the fractional advancement 34%, with a pulse compression of 8% and a secondary-to-main peak amplitude ratio of about 3%.

The theoretical model here presented is valid for MZI operative at any frequency range. As an example, it has been applied to both the optical and RF ranges. In the first case, exact numerical simulations were performed in an MZI designed to advance a pulse centered at 1.55 $\mu$m. In the second case, previously reported experimental results on a coaxial cable MZI have been successfully interpreted.

## ACKNOWLEDGMENTS

Financial support from the Ministerio de Economía y Competitividad (Spain) and Fondos FEDER, through Project No. FIS2012-39158-C02-02, is acknowledged.

[1] L. Thévenaz, Nat. Photonics **2**, 474 (2008).
[2] R. S. Tucker, P. C. Ku, and C. J. Chang-Hasnain, J. Lightwave Technol. **23**, 4046 (2005).
[3] H. N. Yum, M. E. Kim, Y. J. Jang, and M. S. Shahriar, Opt. Express **19**, 6705 (2011).
[4] M. S. Shahriar, G. S. Pati, R. Tripathi, V. Gopal, M. Messall, and K. Salit, Phys. Rev. A **75**, 053807 (2007).
[5] H. Wen, M. Terrel, S. Fan, and M. Digonnet, IEEE Sensors J. **12**, 156 (2012).
[6] Z. Shi, R. W. Boyd, D. J. Gauthier, and C. C. Dudley, Opt. Lett. **32**, 915 (2007).
[7] L. Brillouin, *Wave Propagation and Group Velocity* (Academic, New York, 1960).
[8] A. A. Govyadinov and V. A. Podolskiy, Phys. Rev. Lett. **97**, 223902 (2006).
[9] M. S. Bigelow, N. N. Lepeshkin, and R. W. Boyd, Science **301**, 200 (2003).
[10] L. V. Hau, S. E. Harris, Z. Dutton, and C. H. Behroozi, Nature (London) **397**, 594 (1999).
[11] D. Wei, U. Bortolozzo, J. P. Huignard, and S. Residori, Opt. Express **21**, 19544 (2013).
[12] A. Schweinsberg, N. N. Lepeshkin, M. S. Bigelow, R. W. Boyd, and S. Jarabo, Europhys. Lett. **73**, 218 (2006).
[13] M. González-Herráez, K. Y. Song, and L. Thévenaz, Appl. Phys. Lett. **87**, 081113 (2005).

[14] J. Sharping, Y. Okawachi, and A. L. Gaeta, Opt. Exp. **13**, 6092 (2005).
[15] E. Cabrera-Granado and D. J. Gauthier, Opt. Pura Apl. **41**, 313 (2008).
[16] J. F. Galisteo-López, M. Galli, A. Balestreri, M. Patrini, L. C. Andreani, and C. López, Opt. Express **15**, 15342 (2007).
[17] T. Baba, Nat. Photonics **2**, 465 (2008).
[18] S. Longhi, M. Marano, P. Laporta, and M. Belmonte, Phys. Rev. E **64**, 055602(R) (2001).
[19] G. Nimtz, IEEE J. Sel. Top. Quantum Electron. **9**, 79 (2003).
[20] M. Mojahedi, K. J. Malloy, G. V. Eleftheriades, J. Woodley, and R. Y. Chiao, IEEE J. Sel. Top. Quantun Electron. **9**, 30 (2003).
[21] A. Sánchez-Meroño, J. Arias, and M. M. Sánchez-López, IEEE J. Quantum Electron. **46**, 546 (2010).
[22] A. Haché and L. Poirier, Phys. Rev. E **65**, 036608 (2002).
[23] J. N. Munday and W. M. Robertson, Appl. Phys. Lett. **83**, 1053 (2003).
[24] W. M. Robertson, J. Ash, and J. M. McGaugh, Am. J. Phys. **70**, 689 (2002).
[25] J. Arias, A. Sánchez-Meroño, M. M. Sánchez-López, and I. Moreno, Phys. Rev. A **85**, 033815 (2012).
[26] A. Sánchez-Meroño, M. M. Sánchez-López, J. Arias, J. A. Davis, and I. Moreno, Proc. SPIE **7716**, 77161Y (2010).
[27] G. Singh, V. Janyani, and R. P. Yadav, Optica Applicata **42**, 613 (2012).
[28] S. Khalfallah, P. Dubreuil, R. Legros, C. Fontaine, A. Munoz-Yagüe, B. Beche, H. Porte, R. Warno, and M. Karpierz, Opt. Comm. **167**, 67 (1999).
[29] H. Porte, V. Gorel, S. Kiryenko, J. P. Goedgebuer, W. Daniau, and P. Blind, J. Lightwave Technol. **17**, 229 (1999).
[30] C. Cuadrado-Laborde, Opt. Quantum Electron. **40**, 983 (2008).
[31] E. H. Boudouti, N. Fettouhi, A. Akjouj, B. Djafari-Rouhani, A. Mir, J. O. Vasseur, L. Dobrzynski, and J. Zemmouri, J. Appl. Phys. **95**, 1102 (2004).
[32] W. M. Robertson, J. Pappafotis, P. Flannigan, J. Cathey, B. Cathey, and C. Klaus, Appl. Phys. Lett. **90**, 014102 (2007).
[33] M. M. Sánchez-López, A. Sánchez-Meroño, J. Arias, J. A. Davis, and I. Moreno, Appl. Phys. Lett. **93**, 074102 (2008).
[34] A. Brimont, A. M. Gutierrez, M. Aamer, D. J. Thomson, F. Y. Gardes, J. M. Fedeli, G. T. Reed, J. Martí, and P. Sanchís, IEEE Photon. J. **4**, 1306 (2012).
[35] Z. Shi and R. W. Boyd, J. Opt. Soc. Am. B **25**, 136 (2008).
[36] M. Centini, C. Sibilia, M. Scalora, G. D'Aguanno, M. Bertolotti, M. J. Bloemer, C. M. Bowden, and I. Nefedov, Phys. Rev. E **60**, 4891 (1999).
[37] L. G. Wang and S. Y. Zhu, Opt. Lett. **31**, 2223 (2006).
[38] G. M. Gehring, R. W. Boyd, A. L. Gaeta, D. J. Gauthier, and A. E. Willner, J. Lightwave Technol. **26**, 3752 (2008).
[39] R. W. Boyd and P. Narum, J. Mod. Opt. **54**, 2403 (2007).